Theoretical Modeling and Analysis of Blue Laser Characteristics of Continuous-Wave Single-Wavelength Two-Photon Pumped Rb-Vapor Laser

Yanhui Ji, Yang He, Haohua Wan, Jiamin Wang, and Fei Chen

***Abstract*— Based on an analysis of kinetic processes in the continuous-wave (CW) single-wavelength two-photon pumped Rb-vapor laser (Rb-TPAL), a three-dimensional computational model is established using the rate equation. Based on the application of the model to cavity-enhanced Rb-TPAL [Yuan *et al.*, *Optics Express* 29, 4858 (2021)], the calculated and measured dependences of the laser power on the pump power show good agreement. We simulate the Rb-TPAL pumped by a high-power CW laser diode and analyze the effects of temperature, vapor cell length, pump waist, vapor cell transmission, and output mirror reflectance on the characteristics of the blue laser. The results suggest that the output power and efficiency of blue laser can be improved by optimizing the above parameters; however, the particles in the $5^2D_{5/2}$ level face difficulty to transition to the $6^2P_{3/2}$ level, and this limits the further improvement of blue laser efficiency; therefore, an approach is proposed to improve the efficiency of Rb-TPAL. This study can be useful for designing a two-photon pumped alkali metal laser with high-power output.**

***Index Terms*— Alkali vapor laser, two-photon absorption, infrared laser, blue laser, rate equation.**

I. Introduction

TWO-PHOTON pumped alkali vapor lasers (TPALs) extract near-infrared pump energy and convert it to blue and mid-infrared dual-band laser output that have a broad range of applications in laser communication, photoelectric countermeasures, remote sensing surveys, and laser spectroscopy [1]–[4]. TPALs are divided into single-wavelength and dual-wavelength excitation systems that use single-wavelength or dual-wavelength pump light, respectively, to excite alkali atoms to the corresponding high-energy levels via two-photon absorption. Dual-wavelength excitation TPALs are necessary for combining the two pump beams and adjusting the polarization of the pump light; thus, the realization method is complicated. Single-wavelength excitation TPALs do not require any complicated optical adjustment to meet the phase-matching condition or any complex pump laser system; therefore, single-wavelength excitation TPALs have a more compact structure and have attracted considerable research interest in the recent years.

In terms of theoretical research, in the early stages, the absorption cross-section was defined by Marinescu *et al.* on the basis of the absorption coefficient, by solving the state function based on the Hamiltonian [5]. The two-photon ionization rate of an alkali atom was accurately calculated using the perturbation formula of the second-order transition rate by Bebb *et al.* [6]. The Doppler-free (1st order) two-photon transition probability was calculated using the second-order perturbation theory proposed by Grynberg *et al.* [7]. In addition, the inelastic collisions of alkali metal atoms and oscillator strengths were theoretically calculated [8], [9]. Considering the hyperfine structures of Rb, the third-order susceptibility, and hyperfine line strength, our group used a set of coupled wave equations to calculate the Rb two-photon absorption cross-section [10]. The threshold theory model was developed based on a system of coupled wave equations [11]. The graphical method was used to describe the TPAL non-coincident angular phase matching, and the graphical visualization shows the relationship of the light vectors [12]. However, there is no public report on theoretical models for simulating the output characteristics of TPAL.

In experiment, TPALs usually use pulsed lasers as the pump source because the high peak power can easily realize the pump intensity threshold of single-wavelength two-photon absorption. The two-photon absorption processes of Na, K, Rb, and Cs were realized using a single-wavelength pulsed dye laser and blue light and infrared light were generated [13]–[16]. Recently, Cao *et al.* proposed a Rb-TPAL pumped by a dye laser at 778.1 nm. A blue laser at 420 nm was realized, and the conversion efficiency exceeded 1% [17]. Gai *et al.* used 767.2-nm single-wavelength pulsed dye laser

Manuscript received September 16, 2021; revised November 12, 2021 and December 2, 2021; accepted December 9, 2021. Date of publication December 15, 2021; date of current version January 10, 2022. This work was supported in part by the National Key R&D Program of China under Grant 2018YFE0203201, in part by the National Natural Science Foundation of China under Grant 61975203 and Grant 62005274, in part by the Open Fund Project of the State Key Laboratory of Laser and Material Interaction under Grant SKLLIM1815. *(Corresponding author: Yang He.)*

Yanhui Ji, Haohua Wan, and Jiamin Wang are with the State Key Laboratory of Laser Interaction with Matter, Changchun Institute of Optics, Fine Mechanics and Physics, Chinese Academy of Sciences, Changchun, Jilin 130033, China, and also with the University of Chinese Academy of Sciences, Beijing 100049, China (e-mail: jiyanhui18@mails.ucas.ac.cn; wanhaohua19@mails.ucas.ac.cn; wangjiamin20@mais.ucas.ac.cn).

Yang He and Fei Chen are with the State Key Laboratory of Laser Interaction with Matter, Changchun Institute of Optics, Fine Mechanics and Physics, Chinese Academy of Sciences, Changchun, Jilin 130033, China (e-mail: heyang_3g@126.com; feichenny@126.com).

Color versions of one or more figures in this article are available at https://doi.org/10.1109/JQE.2021.3135880.

Digital Object Identifier 10.1109/JQE.2021.3135880

to pump Cs-vapor TPAL(Cs-TPAL) that output the laser at 387.7 nm and 455.6 nm with the conversion efficiencies of 0.08% and 0.03%, respectively. They also found that introducing the mid-infrared laser at 2.42 μm can enhance the intensity of the laser at 455.6 nm and suppress the laser intensity at 387.7 nm [18]. The above pulse pump source is primarily a dye laser that makes it difficult to achieve high-power laser output; therefore, it is difficult to obtain high-power laser output using TPALs pumped by pulsed lasers. For high-power laser output of TPAL, high-power laser diodes (LDs) can be used as the pump sources. Several improvements have been made to the single-wavelength TPAL using low-power continuous-wave (CW) LD. Brekke *et al.* used a single narrow external cavity diode laser combined with a tapered amplifier system to produce a CW pump laser with a power of 1.131 W at 778 nm, locked to the two-photon $5^2S_{1/2}$–$5^2D_{5/2}$ transition in Rb. With CW pumping, Rb-vapor TPAL (Rb-TPAL) generated ~40-μW blue laser at 420 nm [19]. Subsequently, they used a ring cavity to increase the pump intensity in the Rb-vapor cell, and a 420-nm laser with a power of 1.9 mW was obtained that was 50 times the power achievable without the cavity [20]. Yuan *et al.* demonstrated a 778-nm single-wavelength CW LD-pumped Rb-TPAL, and a blue laser at 420 nm with 3.3-mW power, was generated through the cavity-enhanced process. The beam quality M^2 factors were ~1.117 and ~1.179 along the horizontal and vertical directions, respectively [21]. The above experiments show that CW LD-pumped TPALs can provide blue laser output; therefore, CW high-power LD-pumped TPALs are expected to realize high-power blue laser output. Note that for Rb-TPALs, blue light at 420 nm was produced along with mid-infrared light in the 5-μm band. However, the window material of the Rb-vapor cell is mainly quartz or pyrex glass [18], [20] that has a strong absorption of 5-μm mid-infrared laser. Therefore, it is difficult to generate a mid-infrared laser [22], [23], and the aforementioned Rb-TPALs only achieved a blue laser output.

Against this backdrop, in this study, we developed a three-dimensional analytic theoretical model based on the rate equation and simulated the blue laser characteristics of single-wavelength pumped Rb-TPALs for the first time. The theoretical calculation of the dependence of the laser power on the pump power was compared with the experimental results and they were found to be in good agreement. Thereafter the effects of the parameters of the high-power CW LD-pumped Rb-TPAL such as the temperature, vapor cell length, pump waist, vapor cell transmission, and output mirror reflectance on the blue laser power, efficiency, and pumping threshold were investigated. In addition, we ascertained the reason behind the limiting efficiency of Rb-TPAL and proposed an approach to improve the efficiency of Rb-TPAL. Thus the model and simulation results will contribute to the design of high-power TPAL.

II. Computation Method

The typical geometry of an end-pumped Rb-TPAL is shown in Fig.1. The x and y are the coordinate axes of the cross-section of the alkali cell and the coordinate origin at the center of the cross-section. The z-axis is parallel to the pump and laser optical axis, with the left end of the vapor cell as the coordinate origin, and the direction of the pump laser is positive. A CW laser with a wavelength of 778.1 nm was selected as the pump source. The pump laser beam with intensity I_p was collimated into the resonant cavity composed of plane mirrors M1 and M2. The blue laser intensity I_L passes through the cell window of the transmission. The blue laser beam circulates inside the cavity as $I_L{}^{\pm}$ (+ indicates the z-axis positive direction, - indicates the z-axis negative direction) and is coupled out as the output laser intensity I_{out} through the output coupler M2 with reflectivity.

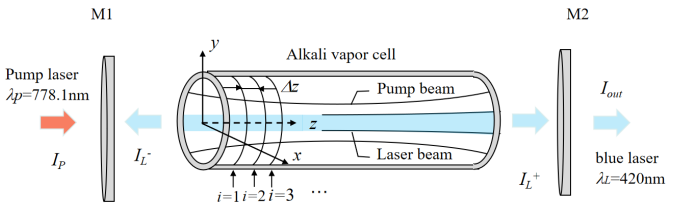

Fig. 1. Schematic of TPAL system.

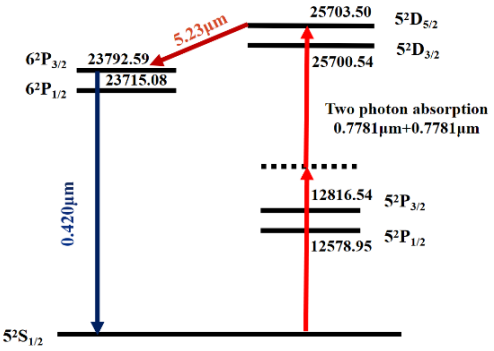

Fig. 2. Schematic of energy levels for Rb-TPAL.

In our model, the alkali vapor cell shown in Fig.1 is filled with ^{87}Rb (27.8%) and ^{85}Rb (72.2%) in their natural abundancies. The Rb energy level and the two-photon absorption process with single-wavelength laser excitation are shown in Fig. 2. The Rb atoms are first excited by two pump photons at 778.1 nm from the $5^2S_{1/2}$ ground state to the upper states 5D ($5^2D_{3/2}$ and $5^2D_{5/2}$ state) by two-photon absorption via the intermediate virtual level marked with the dotted line shown in Fig.2. Because the two-photon absorption cross-section of $5^2S_{1/2}$ to $5^2D_{5/2}$ transition is ~26 times larger than that of the $5^2S_{1/2}$ to $5^2D_{3/2}$ transition, only the former path is considered. Thereafter, the wavelengths of 5.23-μm infrared photons are generated from the $5^2D_{5/2}$ to $6^2P_{3/2}$ transition. Owing to the strong absorption of 5.23-μm infrared light by common cell window materials, oscillation is difficult. Therefore, the stimulated radiation corresponding to the $5^2D_{5/2}$ to $6^2P_{3/2}$ transition was not considered in this model, and only the spontaneous radiation of $5^2D_{5/2}$ to $6^2P_{3/2}$ is considered. Thereafter, due to the transition from the state of $6^2P_{3/2}$ back to the ground state, the blue photon at 420 nm is radiated.

Considering the energy level transition process of pump photons and laser photons in alkali metal atoms, the rate equation of Rb-TPAL can be written as

$$\begin{aligned} \frac{dN_1}{dt} &= \frac{-N_1\sigma_{13}I_p}{h\nu_p}+\frac{(N_2-2N_1)\sigma_{21}I_L}{h\nu_L}+\frac{N_3}{\tau_2}+\frac{N_2}{\tau_1}, \\ \frac{dN_2}{dt} &= \frac{-(N_2-2N_1)\sigma_{21}I_L}{h\nu_L}-\frac{N_2}{\tau_1}+\frac{N_3}{\tau_3}, \\ N_1+N_2+N_3 &= N_0, \end{aligned} \tag{1}$$

where N_1, N_2, and N_3 are the population densities at the levels $5^2S_{1/2}$, $6^2P_{3/2}$, and $5^2D_{5/2}$, respectively, and N_0 is the total population density. h is the Boltzmann constant. $\tau_1$is the radiative lifetime between $6^2P_{3/2}$and $5^2S_{1/2}$, τ_2 is the lifetime of $5^2D_{5/2}$, and τ_3 is the radiative lifetime between $5^2D_{5/2}$ and $6^2P_{3/2}$. ν_L is the laser central frequency, and ν_p is the pump central frequency. σ_{13} is the pump absorption cross section, and σ_{21} is the blue laser emission cross section. Note that Eq. (1) can be applied to any specific spatial position in the gain medium, and N_1, N_2, N_3, I_p, and I_L vary with the space coordinates x, y, and z.

τ_1 and τ_3 can be expressed as follows:

$$\tau_i = \frac{1}{A_{ul}}, \quad i = 1, 3 \tag{2}$$

A_{ul} is the spontaneous radiation rate between energy levels $6^2P_{3/2}$ to $5^2S_{1/2}$ ($u = 2$, $l = 1$) and $5^2D_{5/2}$ to $6^2P_{3/2}$ ($u = 3$, $l = 2$). The spontaneous emission rate between alkali metal atoms can be expressed based on the electric dipole moment as [24]

$$A_{ul} = \frac{g_l}{g_u}\left(\frac{2\pi e^2}{\varepsilon_0 m_e c}\right)\frac{1}{\lambda_{ul}^2}f_{ul} \tag{3}$$

where g_u and g_l are the degeneracy of the levels u and l, respectively. e is the amount of electronic charge, ε_0 is the vacuum permittivity, λ_{ul} is the wavelength corresponding to transition $u \to l$, m_e is the mass of electrons, and c is the speed of light in vacuum, f_{ul} is the oscillator intensity of energy levels $6^2P_{3/2}$–$5^2S_{1/2}$ and $5^2D_{5/2}$–$6^2P_{3/2}$ with the values of 0.0388 and 0.0841, respectively [25].

In steady-state CW operation all the time derivatives in Eq. (1) are zero, and the following solution is obtained.

$$\begin{aligned} N_1 &= \frac{(\frac{1}{\tau_2}+\frac{1}{\tau_1})(\frac{\sigma_{21}I_L}{h\nu_L}+\frac{1}{\tau_1})\cdot N_0}{\frac{1}{\tau_1\tau_2}(\frac{\sigma_{13}I_p}{h\nu_p}+\frac{3\sigma_{21}I_L}{h\nu_L}+\frac{1}{\tau_1})-\frac{\sigma_{13}I_p}{h\nu_p}(-\frac{\sigma_{21}I_L}{h\nu_L}+\frac{1}{\tau_1}+\frac{1}{\tau_2})}, \\ N_2 &= \frac{\frac{\sigma_{13}I_pN_1}{\left(\frac{1}{\tau_1}+\frac{1}{\tau_2}\right)h\nu_p\tau_3}+\frac{2\sigma_{21}I_L}{h\nu_L}}{\frac{\sigma_{21}I_L}{h\nu_L}+\frac{1}{\tau_1}}\cdot N_1, \\ N_0 &= N_1+N_2+N_3, \end{aligned} \tag{4}$$

The saturated laser gain coefficient can be written as

$$g(x, y, z) = \sigma_{21}\left[N_2(x, y, z) - 2N_1(x, y, z)\right] \tag{5}$$

The saturation absorption coefficient can be written as

$$\sigma(x, y, z) = \sigma_{13}N_1 = \sigma_{TAT}I_PN_1(x, y, z) \tag{6}$$

where σ_{TAP} is the two-photon absorption cross section (cm^4/W). Our group derived a calculation formula based on coupled wave equations [10].

The propagation process of the blue laser can be approximated by paraxial approximation to simulate the propagation process of light wave in resonant cavity. In this study, the beam propagation equation was used to calculate the spatial distribution of the single-wavelength pumped Rb-TPAl laser intensity. For the laser propagating in the resonant cavity, the formula for calculating the blue laser amplitude Al is written as [26]

$$2ik_l\frac{\partial A_l(x, y, z)}{\partial z} = \frac{\partial^2 A_l(x, y, z)}{\partial x^2}+\frac{\partial^2 A_l(x, y, z)}{\partial y^2} \tag{7}$$

$$2ik_l\frac{\partial A_l(x, y, z)}{\partial z} = \frac{\partial^2 A_l(x, y, z)}{\partial x^2}+\frac{\partial^2 A_l(x, y, z)}{\partial y^2}+ik_lg(x, y, z)A_l(x, y, z) \tag{8}$$

Eq. (7) and Eq. (8) present the approximate formula of the axis in the free space and the alkali vapor cell, respectively. k_l is the wave number of the blue laser in vacuum.

We can numerically calculate the propagation of the blue laser in the Rb-vapor cell and the free space inside the cavity by solving Eq. (4)–(8). An iterative method is designed to numerically calculate the laser propagation back and forth in the cavity [27]: Along the z-axis of the Rb-vapor cell, the gain medium of TPAL is divided into small volume segments with the length of Δz. The initial value of the effective pump intensity $I_p(x, y, 0)$ is known, and laser intensity $I_L(x, y, 0)$ is chosen arbitrarily. The population density at each energy level is determined by Eqs. (4). The pump intensity $I_p(x, y, \Delta z)$ is obtained by substituting Eq. (6) into (8) (change $g(x, y, z)$ to $\sigma(x, y, z)$ in Eq. (8)). And the laser intensity $I_L(x, y, \Delta z)$ can be computed by substituting Eq. (5) into (8). $I_L(x, y, \Delta z) = I_L{}^+(x, y, \Delta z) + I_L{}^-(x, y, \Delta z)$ is calculated using the complex amplitudes of the two counter-propagating lasers stored in the previous step. The laser intensity between the cell and the mirror can be calculated using Eq. (7). The blue laser is numerically propagated through the cavity for an additional round trip until the values of the pump and laser intensity stabilize. Accordingly, the intensity of the pump light and the blue laser of the Rb-TPAL is obtained.

III. Results and Discussion

In this section, the calculated and measured values of the dependence of the laser power on the pump power are calculated, and the results show a good agreement. We have also simulated the high-power CW LD-pumped Rb-TPAL and examined the influence of the vapor cell temperature, vapor cell length, output mirror reflectivity, vapor cell transmission, vapor cell length, pump beam waist position, and pump power on the blue laser characteristics in the presence of CW LD-pumped Rb vapor. Finally, we propose a solution to improve the efficiency of Rb-TPAL.

A. Comparion With the Experiment

We modeled single-wavelength pumped Rb-TPAL and compared the calculated results with the experimental results provided by Yuan *et al.* [21]. The schematic setup of the simulation is illustrated in Fig. 3. The pump laser is a

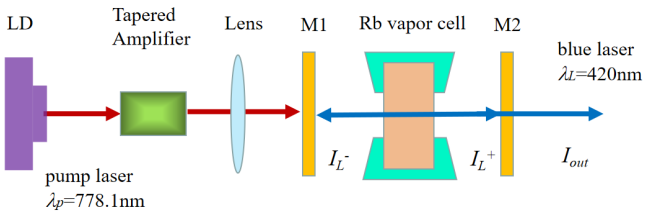

Fig. 3. Schematic diagram of TPAL.

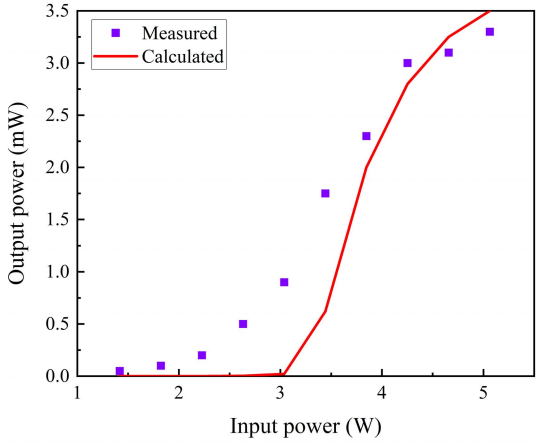

Fig. 4. Measured [21] and calculated results for the dependence of the output laser power on the pump power.

778.1-nm CW LD with an output power of up to 1.25 W. The pump laser is focused on the Rb-vapor cell in the cavity through a lens. In Ref. [21], a ring cavity with four mirrors was used; however the specific parameters were not provided. We used a flat - flat cavity instead of a ring cavity to simplify the simulation.

The main conditions used in the calculations are shown in Table I. Note that the circulating power through a ring cavity was 4.05 times the input power in Ref. [21], whereas the pump power was directly set to the circulating power in our model. Fig. 4 shows the results, where the output power is plotted as a function of the pump power. The calculated output power is close to the experimental results. A comparison of the calculated results with the measurement, shows that for a relatively high pump power (>3.8 W) the model predicted extremely close values of the laser power, implying that our model has an applicability in single-wavelength pumped Rb-TPAL. When pump power is less than 3.8 W, the measured threshold and output power are higher than the calculated ones. Because in our model, the MIR light at 5.23 μm is not considered, but it is expected to generate 5.23-μm spontaneous emission and amplified spontaneous emission (ASE) in the experiment. The MIR light can increase the transition rate from $5^2D_{5/2}$ to $6^2P_{3/2}$ that could decrease the blue light threshold and improve the blue laser power when pump power is low.

TABLE I
PARAMETERS USED IN THE EXPERIMENT AND SIMULATION

Symbol	Experiment [21]	Simulation (this study)
Pump central wavelength	778.1 nm	778.1nm
Maximum pump power	1.25W (Actual) 5.06W(Equal)	5.06W
Pump waist radius	0.19μm	0.19μm
output mirror reflection	92%	92%
vapor cell transmission	80.3%	80.3%
Laser central wavelength	420 nm	420 nm
Rb density	1.35×10^{14}/cm^2	1.35×10^{14}/cm^2
length of Rb-vapor cell	--	4cm (estimated)
Two-photon absorption cross section	--	1.4×10^{-19} cm^4/W [10]
Stimulated absorption cross section	--	Defined $I_P\times\sigma_{TPT}$ [28]
$6^2P_{3/2}$ – $5^2S_{1/2}$ radiative lifetime	--	335.6×10^{-9} s (Calculated)
$5^2D_{5/2}$ radiative lifetime	--	231.5×10^{-9} s [29]
$5^2D_{5/2}$ – $6^2P_{3/2}$ radiative lifetime	--	698.655×10^{-9} s (Calculated)

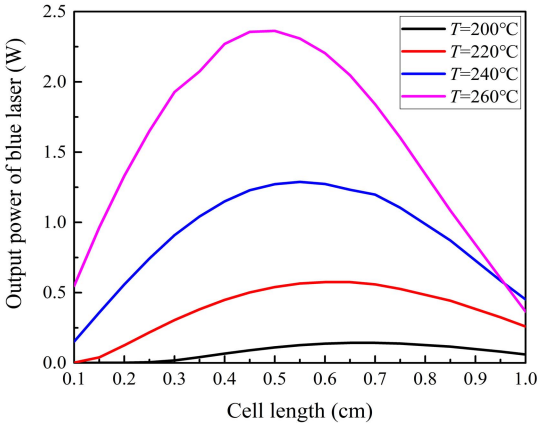

Fig. 5. Output power of blue laser as function of cell length under different temperature conditions.

B. Rb-TPAL Pumped by High-Power CW LD

In this section, the theoretical simulation and parameter optimization of a TPAL pumped by a high-power CW fiber-coupled LD are conduction to explore the feasibility of outputting high-power blue laser. The simulation conditions are as follows: pump power is 100 W; core radius and numerical aperture of the pump fiber is 200 μm and 0.22, respectively; pump beam waist radius is 400 μm and the location is in the center of resonant cavity; vapor cell transmission is 95% and output mirror reflectivity is 15%; the vapor cell is 1 cm away from M1 and M2. The other parameters are the same as those in Table I.

1) Influence of Temperature and Length of Rb-Vapor Cell: As shown in Fig. 5, the output power of the blue laser as a function of the cell length (L) at different temperatures (T).

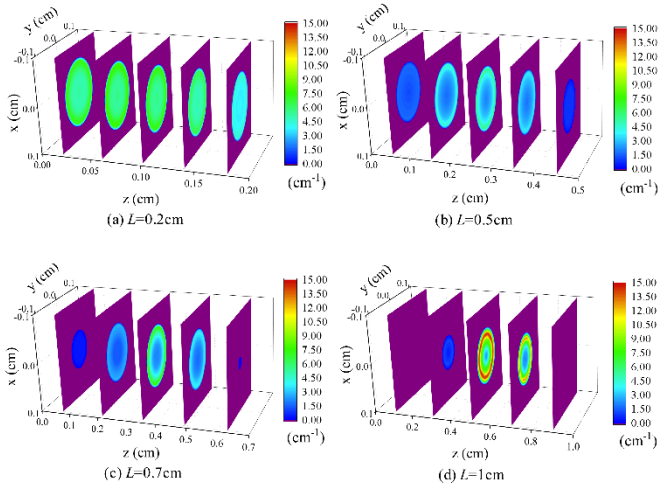

Fig. 6. (a)–(d) Distribution of gain coefficients in the vapor cell under steady state for different cell lengths at 260°C (set negative gain to purple).

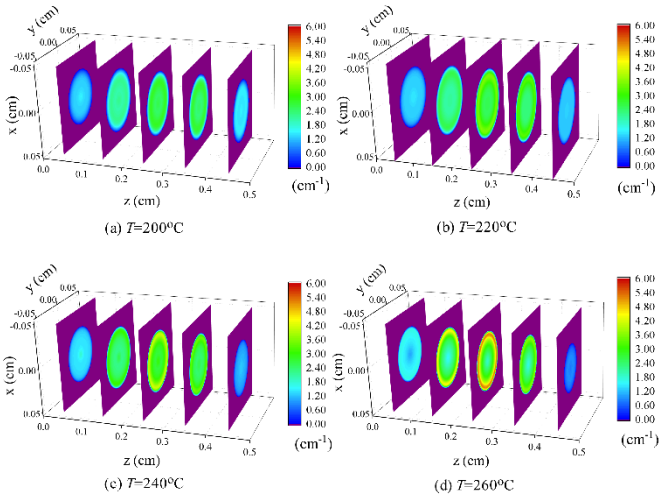

Fig. 7. (a)–(d) Distribution of gain coefficients in the vapor cell at steady state under different temperature when cell length is 0.5cm.

It can be seen that for a certain T of the vapor cell, there is an optimal L that maximizes the blue laser output power. With the increasing T, the optimal vapor cell length decreases, and the corresponding blue laser power increases. When T is 200 °C, 220 °C, 240 °C, and 260 °C, the optimal lengths of the cell are 0.7 cm, 0.6 cm, 0.55 cm, and 0.5 cm, respectively. The corresponding output powers are 0.143 W, 0.575 W, 1.288 W, and 2.362 W, respectively.

The reason behind the optimal L can be understood from Fig. 5. The distribution of the gain coefficients in the cell under steady state is shown in Fig. 6(a)–(d) for $T = 260$ °C and $L = 0.2$ cm, 0.5 cm, 0.7 cm, and 1 cm. When $L \leq 0.5$ cm, the gain coefficient of $L = 0.5$ cm is relatively small, compared with that for $L = 0.2$ cm; however, L is relatively large. Blue light can fully absorb the pump light in the vapor cell, and the total gain is high; thus, the blue laser output power also increases. When $L > 0.5$ cm, the pump is fully absorbed at the front end of the vapor cell, and the pump laser power decreases rapidly in the right half that causes the Rb atom to be unable to absorb sufficient pump light to be excited. The blue laser gain changes from a positive value to a negative value, and Rb vapor forms an absorption loss on the blue laser, resulting in a decrease in the blue laser power. The higher the temperature, the shorter the length of the optimal vapor cell because Rb population densities increase with the increase in temperature, and the cell length required to ensure complete absorption of the pump light is shorter; therefore, the optimal length is shorter.

The results in Fig. 5 also show that there is an optimal working temperature for a fixed vapor cell length. When $L <$ 0.95 cm, the output power of the blue laser increases with the increase in temperature. This can be attributed to the distribution of the gain coefficients in the cell under steady state for $L = 0.5$ cm and the temperatures of 200 °C, 220 °C, 240 °C, and 260°C, as illustrated in Fig. 7(a)–(d). As T increases, the concentration of Rb atoms increases, and the gain increases; thus, the blue laser power increases with an increase in the working temperature.

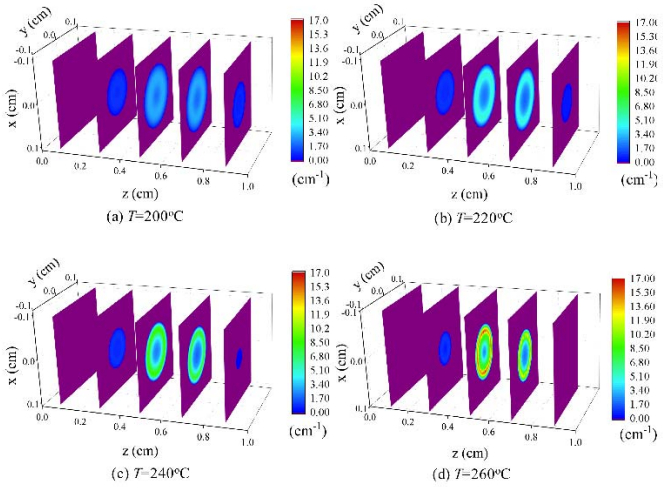

Fig. 8. (a)–(d) Distribution of gain coefficients in the vapor cell at steady state under different temperature when cell length is 1cm.

However, when $L > 0.95$ cm, the optimal temperature becomes 240 °C, as shown in Fig. 8(a)–(d) that illustrate the distribution of the gain coefficients in the cell under steady state for a cell length of 1 cm and T of 200 °C, 220 °C, 240 °C, and 260 °C, respectively. When $T \leq 240$ °C, as T increases, Rb atom concentration increases, and the gain is high; thus, the power of the blue laser increases as the working temperature increases. When the working temperature T is 260 °C, the concentration of Rb atoms becomes extremely high, causing the pump energy to be fully absorbed by the front end of the vapor cell ($z < 0.5$ cm), and the blue laser gain is also higher (when the temperature is 260 °C and maximum gain coefficient is 10.26cm^{-1}), compared with the back end of the vapor cell ($z > 0.5$ cm); as the pump energy is fully absorbed, the power drops rapidly, such that the Rb atoms cannot absorb further pump energy to be excited. The blue laser gain changes from a positive value to a negative value, and Rb vapor instead contributes to the absorption loss of the

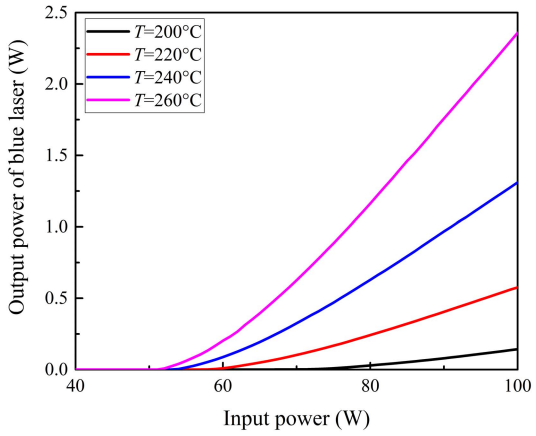

Fig. 9. Output power as function of input power at different temperatures.

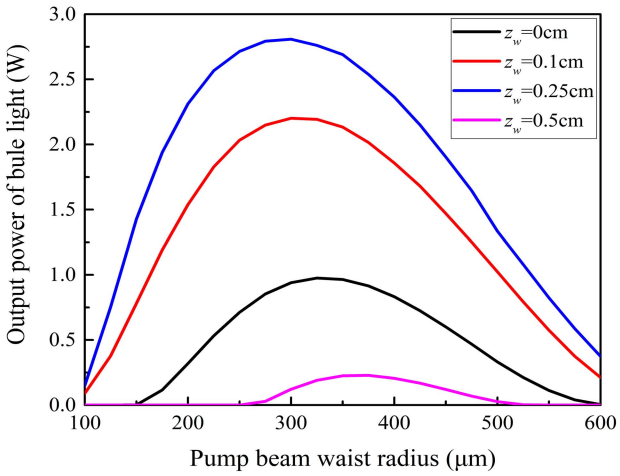

Fig. 10. Output power as a function of the radius of pump waist for different pump beam waist positions.

blue laser that eventually causes the blue laser output power to decrease with the increase in the operating temperature.

Fig. 9 shows the variation of the output power with the input power at different temperatures with the most optimal cell length. The temperatures T are 200 °C, 220 °C, 240 °C and 260 °C, corresponding to the threshold intensity of 1.393×10^4W/cm^2, 1.154×10^4W/cm^2, 1.074×10^4W/cm^2 and 1.036×10^4W/cm^2. With T increasing, the threshold pump intensity decreases. The slope efficiency and conversion efficiency increase with the increase in T. The temperatures of the cell are 200°C, 220°C, 240°C and 260°C, corresponding to the slope efficiency of 0.47%, 1.35%, 2.85% and 4.92%, and the optical-optical conversion efficiencies are 0.14%, 0.57%, 1.31%, and 2.36%, respectively.

2) Influence of Pump Beam Waist Radius and Position: From the above simulation results, the temperature was set to 260°C, the vapor cell length was chosen to be 0.5cm, and the other parameters were the same as mentioned above. We obtain the relationship between the output power of the blue laser as a function of the radius of the pump waist (w_p) under different pump beam waist positions (z_w) along the z-axis.

In the case of LD pumping, the pump beam waist radius and position have a significant effect on the output power. It can be seen from Fig. 10 that when the coordinate of the pump beam waist position z_w on z-axis are 0cm, 0.1cm, 0.25cm, and 0.5cm, the optimal pump waist radius are 325μm, 300μm, 300μm, and 375μm, respectively. The corresponding output powers are 0.98 W, 2.20W, 2.81W, and 0.13 W, respectively. As shown in Fig. 10, it also can be seen that as the pump beam waist moves toward the center of the vapor cell, the output power gradually increases, and the output power is maximum when the pump beam waist is located in the center of the vapor cell ($z_w = 0.25$ cm). as shown in Fig. 11(a)–(d) that illustrate the distribution of the gain coefficients in the cell under steady state for a waist radius $w_p = 300\mu$m and z_w of 0cm, 0.1cm, 0.25cm, and 0.5cm, respectively. The degree of pump and laser mode overlapped can be calculated as 0.14, 0.173, 0.195, 0.14, respectively [30]. When $z_w < 0.25$ cm, the pump light intensity is large in the front end of the vapor cell, the pump energy is fully absorbed and the gain is high. However, as the

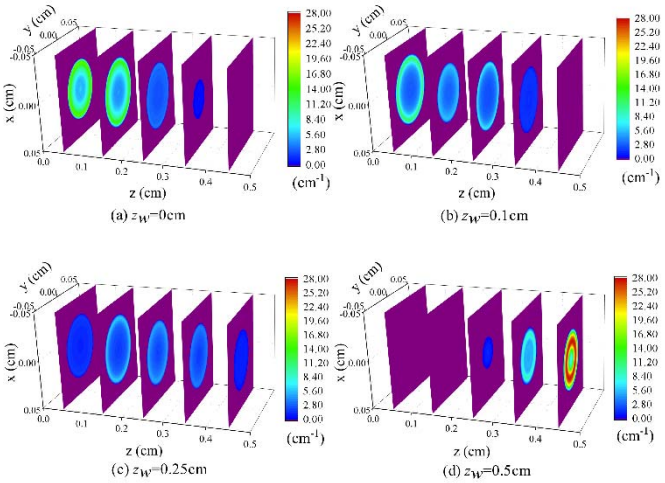

Fig. 11. (a)–(d) Distribution of gain coefficients in the vapor cell at steady state under different pump beam waist radius when waist radius wp = 300μm.

pump energy is fully absorbed, the power drops rapidly, that the Rb atoms cannot absorb further pump energy to be excited. The blue laser gain changes from a positive value to a negative value, which limited blue laser power. When $z_w > 0.25$ cm, the pump light intensity is low in the front end of the vapor cell, Rb atoms cannot to be excited to $5^2D_{5/2}$, the blue laser gain becomes negative value that leads the blue laser power to decrease. When $z_w = 0.25$ cm, the best mode matching can be achieved and the blue laser gain along the vapor cell is all positive, so the blue light output power is the highest.

3) Influence of Output Mirror Reflection and Vapor Cell Window Transmission: From the above simulation, we can obtain the relationship between the output power and the beam waist position and radius. The value of w_p is chosen to be 300μm. The pump beam waist is located at $z_w = 0.25$ cm, and the other parameters are the same as above. In this subsection, we analyze the relationship between the output power of the blue laser and the reflectivity of the output mirror R for different cases of the vapor cell window transmission T_w.

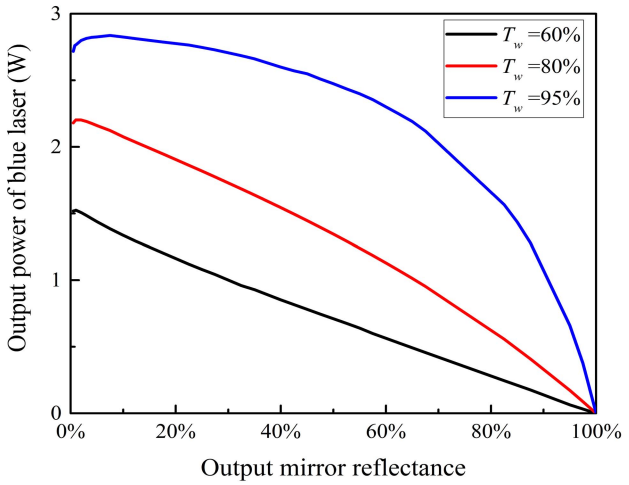

Fig. 12. Output power as function of output mirror reflectance for different vapor cell window transmission.

As shown in Fig.12, the output power of the blue laser increases with an increase in the Rb-vapor cell window transmission. The loss caused by the Rb-vapor cell window can lead to a significant reduction in power; therefore, in the design of single-wavelength TPAL systems, a vapor cell window coated with a transmission-enhancing film is required to keep the window clean. Because of the large gain coefficient in Rb-TPAL, when R is extremely small, the Rb-TPAL can still output blue laser that indicates that the blue laser output can be realized without the resonator cavity that is consistent with the experiment [20]. When T_w is 60%, 80%, and 95%, and the reflectivity of the output mirror is 0.8%, 3%, and 7.5%, the maximum blue laser power is 1.52 W, 2.20 W, and 2.83 W, respectively. This shows that adding the resonator cavity is advantageous to improving the blue laser output power of Rb-TPAL, and the higher the T_w, the greater is the optimal reflectivity of the reflector.

4) Power Scaling: Considering the above simulation results, the simulation conditions are as follows: the vapor temperature is 260 °C, vapor cell window transmission is 95%, output mirror reflectivity is 7.5%, pump beam waist radius is 300 μm, and the pump beam waist is located at the center of the Rb-vapor cell. The following figure shows the relationship between the output power and input power corresponding to the optimal vapor cell length.

It can be seen from Fig. 13(a) that when the pump power is 100 W, 200 W, 300 W, 400 W, and 500 W, the output powers are 2.83 W, 10.76W, 20.60 W, 31.47 W, and 43.64 W, and the optical–optical conversion efficiency is 2.83%, 5.38%, 6.87%, 7.62%, and 8.73%, respectively. Corresponding to the optimal vapor cell length of 0.5 cm, 0.9 cm, 1.2 cm, 1.4 cm, and 1.6 cm, the output power is positively correlated with the input power. Fig. 13(b–d) shows the distribution of the population densities at each energy level in the vapor cell for the pump power of 500 W. It can be seen that the population densities at the pump upper-level $5^2D_{5/2}$ under the steady state are much larger than the laser upper-level $6^2P_{3/2}$ population densities N_2 and ground-state $5^2S_{1/2}$ population densities N_1. This is because in the case of high-power pumping, Rb atoms undergo

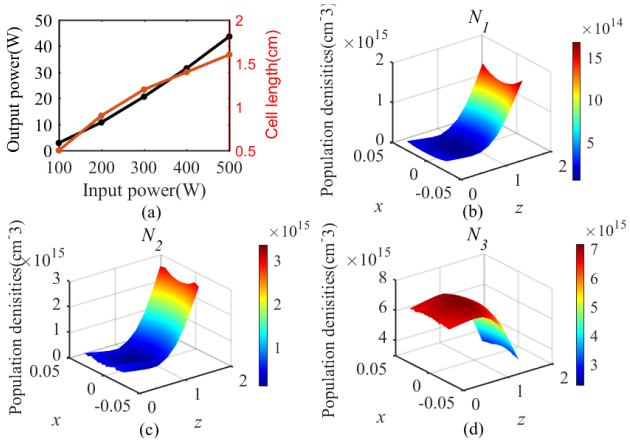

Fig. 13. (a) Output power as a function of the input power and vapor cell length (b–d) distribution of population densities in the vapor cell under steady state.

a large number of transitions to the $5^2D_{5/2}$ energy level after absorbing the pump laser, and the spontaneous emission rate between $5^2D_{5/2}$ and $6^2P_{3/2}$ is relatively small that makes it difficult to cause a considerable number of particles in the $5^2D_{5/2}$ level to transition to the $6^2P_{3/2}$ level, resulting in a lower blue laser output power. Increasing the 5.23-μm mid-infrared laser is expected to increase the transition rate from $5^2D_{5/2}$ to $6^2P_{3/2}$ that not only improves the transition rate from $5^2D_{5/2}$ to $6^2P_{3/2}$ to increase the blue laser output power, but also amplifies the mid-infrared laser. Simultaneously, the vapor cell window material needs to be replaced with magnesium fluoride (MgF_2), sapphire, or other materials with high transmission of mid-infrared laser. A similar method of introducing mid-infrared light to improve the blue laser output power of Cs-TPAL was experimentally tested in Ref. [18]. In the follow-up research, a simulation analysis of the mechanism of mid-infrared light will be performed for improving the blue laser output power of the TPAL.

IV. Conclusion

In this study, we use the rate equation to establish a single-wavelength CW Rb-TPAL three-dimensional theoretical model for the first time to analyze the effect of each parameter on the characteristics of blue laser at 420 nm. Firstly, based on the theoretical model applied in Ref. [21], the calculated results are in good agreement with the measurements. A simulation analysis of Rb-TPAL pumped by high-power CW LD at 778.1 nm is performed, and the following conclusions are obtained. An optimal combination of temperature and cell length can maximize the output power of the blue laser. With an increase in the optimal temperature, the corresponding cell length decreases, and a higher output power is achieved. The pump beam waist has a significant effect on the output power. When the pump beam waist is located on the center of the vapor cell, the Rb-TPAL realizes the maximum blue laser power upon selection of the appropriate pump beam waist radius. The output power of the blue laser increases with the increase in vapor cell window transmission, and compared with the case without the resonator cavity, the addition of the resonator cavity is advantageous to the improvement of

the blue laser power, and there is an optimal reflectivity of the output mirror that maximizes the blue laser output power. Finally, we use the established relationship to obtain the optimization results: when the pumping power reaches 500 W, the output power reaches up to 43.64 W and the efficiency is 8.73%; the efficiency of the blue laser is low because of the population aggregation of Rb atoms on the upper energy level $5^2D_{5/2}$. It is speculated that this problem can be solved by introducing mid-infrared light to increase the transition rate from $5^2D_{5/2}$ to $6^2P_{3/2}$. In conclusion, we believe that the model and simulation results can provide an effective way to design a high power TPAL system. In the next simulation, the mid-infrared laser factor will be considered. Furthermore, the temperature distribution, pump linewidth and the buffer gas will also be considered to optimize the theoretical model.

REFERENCES

[1] M. F. Ali, D. N. K. Jayakody, Y. A. Chursin, S. Affes, and S. Dmitry, "Recent advances and future directions on underwater wireless communications," *Arch. Comput. Methods Eng.*, vol. 27, no. 5, pp. 1379–1412, Nov. 2020.

[2] V. Karaganov, M. Law, M. Kaesler, D. G. Lancaster, and M. R. Taylor, "Engineering development of a directed IR countermeasure laser," *Proc. SPIE*, vol. 5615, pp. 48–53, Dec. 2004.

[3] M. Vlk *et al.*, "Extraordinary evanescent field confinement waveguide sensor for mid-infrared trace gas spectroscopy," *Light: Sci. Appl.*, vol. 10, no. 1, pp. 1–7, Dec. 2021.

[4] J. Kasparian and J.-P. J. Wolf, "Physics and applications of atmospheric nonlinear optics and filamentation," *Opt. Exp.*, vol. 16, no. 1, pp. 466–493, 2008.

[5] M. Marinescu, V. Florescu, and A. Dalgarno, "Two-photon excitation of the 5 ^2D states of Rubidium," *Phys. Rev. A, Gen. Phys.*, vol. 49, no. 4, p. 2714, 1994.

[6] H. B. Bebb, "Quantitative theory of the two-photon ionization of the alkali atoms," *Phys. Rev.*, vol. 149, no. 1, p. 25, 1966.

[7] G. Grynberg and B. Cagnac, "Doppler-free multiphotonic spectroscopy," *Rep. Prog. Phys.*, vol. 40, no. 7, p. 791, 1977.

[8] J. Pascale, "Oscillator strengths for $S--S$ and $S--D$ induced dipole transitions in alkali–rare gas systems," *J. Chem. Phys.*, vol. 67, no. 1, pp. 204–209, 1977.

[9] D. McGillis and L. Krause, "Inelastic collisions between excited alkali atoms and molecules. I. Sensitized fluorescence and quenching in Cs-N_2 and Cs-H_2 systems," *Phys. Rev.*, vol. 153, no. 1, p. 44, 1967.

[10] H. Yu *et al.*, "Theoretical modeling and analysis on the absorption cross section of the two-photon excitation in Rb," *Opt. Exp.*, vol. 26, no. 13, pp. 17254–17263, Jun. 2018.

[11] H. Yu, F. Chen, Q. Pan, Y. He, and J. Xie, "Modeling and analysis of the pumping threshold characteristics in one-color two-photon excited Cs vapor," *IEEE J. Quantum Electron.*, vol. 56, no. 2, pp. 1–6, Apr. 2020.

[12] H. Yu, F. Chen, Y. He, Q. Pan, D. Yu, and J. Xie, "Nonlinear phase matching in parametric four-wave mixing process of Cs vapor," *Optik*, vol. 205, Mar. 2020, Art. no. 163583.

[13] W. Hartig, "Two-photon resonant four-wave mixing in atomic sodium vapour," *Appl. Phys.*, vol. 15, no. 4, pp. 427–432, Apr. 1978.

[14] P.-L. Zhang and A. L. Schawlow, "Two-photon resonant optical processes in atomic potassium," *Can. J. Phys.*, vol. 62, no. 12, pp. 1187–1197, Dec. 1984.

[15] S. M. Hamadani, J. A. D. Stockdale, R. N. Compton, and M. S. Pindzola, "Two-photon resonant four-wave mixing and multiphoton ionization of cesium in a heat-pipe oven," *Phys. Rev. A, Gen. Phys.*, vol. 34, no. 3, pp. 1938–1943, Sep. 1986.

[16] Y. J. Chan and W. T. Luh, "Six-wave mixing near-infrared emissions in Rubidium vapor," *Chin. J. Phys.*, vol. 33, no. 3, pp. 247–261, 1995.

[17] R. Cao *et al.*, "Efficient generation of collimated frequency upconversion blue light in Rubidium vapor," *Chin. Opt. Lett.*, vol. 13, no. 12, 2015, Art. no. 121903.

[18] B. Gai *et al.*, "Modulation of a double-line frequency up-conversion process in cesium vapor," *Appl. Phys. B, Lasers Opt.*, vol. 122, no. 6, p. 165, Jun. 2016.

[19] E. Brekke and L. Alderson, "Parametric four-wave mixing using a single Cw laser," *Opt. Lett.*, vol. 38, no. 12, pp. 2147–2149, Jun. 2013.

[20] E. Brekke and S. Potier, "Optical cavity for enhanced parametric four-wave mixing in Rubidium," *Appl. Opt.*, vol. 56, no. 1, pp. 46–49, Jan. 2017.

[21] J. Yuan, H. Liu, L. Wang, L. Xiao, and S. Jia, "Coherent 420 nm light generated by the cavity-enhanced four-wave mixing process in Rb vapor," *Opt. Exp.*, vol. 29, no. 4, pp. 4858–4865, 2021.

[22] A. M. Akulshin, D. Budker, and R. J. McLean, "Parametric wave mixing enhanced by velocity-insensitive two-photon excitation in Rb vapor," *J. Opt. Soc. Amer. B, Opt. Phys.*, vol. 34, no. 5, pp. 1016–1022, May 2017.

[23] R. F. Offer, J. W. C. Conway, E. Riis, S. Franke-Arnold, and A. S. Arnold, "Cavity-enhanced frequency up-conversion in Rubidium vapor," *Opt. Lett.*, vol. 41, no. 10, pp. 2177–2180, May 2016.

[24] O. Axner, J. Gustafsson, N. Omenetto, and J. D. Winefordner, "Line strengths, A-factors and absorption cross-sections for fine structure lines in multiplets and hyperfine structure components in lines in atomic spectrometry—A user's guide," *Spectrochim. Acta B, At. Spectrosc.*, vol. 59, no. 1, pp. 1–39, 2004.

[25] B. Warner, "Atomic oscillator strengths-III. Alkali-like spectra," *Monthly Notices Roy. Astronomical Soc.*, vol. 139, no. 1, pp. 115–128, Mar. 1968.

[26] H. Shu and M. Bass, "Three-dimensional computer model for simulating realistic solid-state lasers," *Appl. Opt.*, vol. 46, no. 23, pp. 5687–5697, 2007.

[27] H. Shu, Y. Chen, M. Bass, J. F. Monjardin, and J. Deile, "Numerical modeling of alkali vapor lasers," *Opt. Exp.*, vol. 19, no. 21, pp. 19875–19885, Oct. 2011.

[28] J. E. Gallagher, "Optically pumped atomic Rubidium lasers: Two photon and exciplex excitation mechanisms," Air Force Inst. Technol., OH, USA, Tech. Rep., 2013, ch. 2.

[29] C. E. Theodosiou, "Lifetimes of alkali-metal—Atom Rydberg states," *Phys. Rev. A, Gen. Phys.*, vol. 30, no. 6, p. 2881, 1984.

[30] A. Sennaroglu and B. Pekerten, "Experimental and numerical investigation of thermal effects in end-pumped Cr/sup 4+/:Forsterite lasers near room temperature," *IEEE J. Quantum Electron.*, vol. 34, no. 10, pp. 1996–2005, Oct. 1998.

Yanhui Ji was born in 1996. She received the bachelor's degree from the Changchun University of Science and Technology in 2018. She is currently pursuing the degree in optical engineering with the Changchun Institute of Optics, Fine Mechanics and Physics, Chinese Academy of Sciences, China, and the University of Chinese Academy of Sciences, China. She is mainly engaged in the research of alkali metal lasers.

Yang He was born in 1988. He received the master's degree from Tianjin University in 2013 and the Ph.D. degree from the University of Chinese Academy of Sciences in 2020. He is currently with the State Key Laboratory of Laser Interaction With Matter, Changchun Institute of Optics, Fine Mechanics and Physics, Chinese Academy of Sciences. He is currently an Assistant Researcher. He is mainly engaged in the research of gas laser and solid laser.

Haohua Wan was born in 1996. He received the bachelor's degree from Tianjin University in 2019. He is currently pursuing the degree in optical engineering with the Changchun Institute of Optics, Fine Mechanics and Physics, Chinese Academy of Sciences, China, and the University of Chinese Academy of Sciences, China. He is mainly engaged in the research of alkali metal lasers.

Jiamin Wang was born in 1995. She received the bachelor's degree from Inner Mongolia University in 2018. She is currently pursuing the degree in optical engineering with the Changchun Institute of Optics, Fine Mechanics and Physics, Chinese Academy of Sciences, China, and the University of Chinese Academy of Sciences, China. She is mainly engaged in the research of laser applications.

Fei Chen was born in 1982. He received the Ph.D. degree from the Harbin Institute of Technology in 2011. He is currently with the State Key Laboratory of Laser Interaction With Matter, Changchun Institute of Optics, Fine Mechanics and Physics, Chinese Academy of Sciences. He is also a Professor and the Doctoral Supervisor. He is mainly engaged in the research of high-power gas lasers and their applications.